ISSN: 2414-1895 DOI: 10.6919/ICJE.202603_12(3).0028

Active Disturbance Rejection Controller for Servo System Current Loop based on Linear Extended State Observer

Xiuwen Shan[1], Lixiang Sun[1], Yi Zhang[2], and Hanpei Wei[2, a]

[1] Joint Technology Transfer Center of Yancheng Polytechnic College, Yancheng Polytechnic College, Yancheng 224005, China

[2] School of Automation, Jiangsu University of Science and Technology, Zhenjiang 212003, China

[a]1506089882@qq.com

Abstract

This paper first introduces the advantages of the active disturbance rejection controller and the standard active disturbance rejection controller model. The active disturbance rejection controller is applied to the current loop of the permanent magnet AC servo control system, and a current loop active disturbance rejection controller composed of a linear extended state observer and a state error feedback rate is designed. It is introduced into the current loop of the servo system for performance analysis. Secondly, in terms of dynamic response, improving the current feedback and updating the PWM duty cycle can enhance the dynamic performance. Finally, the anti-interference performance of the current loop in the AC servo system was analyzed. The experimental results verified the robustness of the new servo system current loop active disturbance rejection controller to motor parameter perturbation.

Keywords

Current Loop Active Disturbance Rejection Controller; Linear Extended State Observer; State Error Feedback Rate; Parameter Perturbation.

1. Introduction

Based on the quality requirements of high-performance permanent magnet synchronous motor (PMSM) servo systems, there are issues in permanent magnet AC servo systems that need to be addressed: the dynamic response and robustness of the servo system under nonlinear factors and uncertain disturbances, mainly including internal parameter perturbations [1,2]. Firstly, the PMSM body system is a nonlinear, multivariable, and strongly coupled system [3]. Although it can be controlled as a DC motor through vector decoupling control, there is still current coupling between the d-axis and q-axis. Under sudden changes in external load and heavy load conditions, this coupling term can degrade the decoupling control performance of the system, affect system stability, and further reduce the dynamic response performance of the servo system. Secondly, the mechanical parameters of the PMSM body, such as motor stator resistance, inductance, and rotor flux linkage, are sensitive to the ambient temperature. The heating of the motor under different operating conditions can cause certain perturbations in these parameter values, leading to changes in the motor body model. Considering that the current inner loop control of traditional PMSM servo systems is usually based on the mathematical model of the body, the dynamic response capability of the current inner loop under internal parameter perturbations of the motor will be greatly compromised, which can seriously destabilize the inner loop system and cause current oscillation phenomena.

ISSN: 2414-1895 DOI: 10.6919/ICJE.202603_12(3).0028

Due to the variable coupling nonlinearity, model uncertainty, unpredictable parameter perturbations, and external load disturbances in permanent magnet synchronous motor (PMSM) systems, traditional linear control methods, such as PI control, have been unable to meet the increasingly high quality requirements of high-performance PMSM servo systems as China's industrial automation requirements have increased. In order to improve the control performance of PMSMs, many nonlinear control methods have been developed in the field of motor control in recent years, such as sliding mode variable structure control [4], adaptive control [5], backstepping control [6], fuzzy control [7], and active disturbance rejection control [8]. These control methods have improved the control performance of motors from different perspectives and enhanced the disturbance rejection capability of servo systems.

In this paper, the Active Disturbance Rejection Controller (ADRC) is applied to the current loop of a permanent magnet AC servo control system. A current loop ADRC consisting of a linear extended state observer and a state error feedback rate is designed. Afterwards, the performance of the current loop with the controller is analyzed. In terms of dynamic response, the dynamic performance is improved by improving the current feedback and the update method of the PWM duty cycle. Finally, the disturbance rejection performance of the current loop is analyzed.

2. Standard Active Disturbance Rejection Controller Model

The standard Active Disturbance Rejection Controller (ADRC) consists of a Tracking Differentiator (TD), an Extended State Observer (ESO), and a Linear State Error Feedback Control Law (LSEF). These three components are independent of each other, and can be designed separately during the controller design process.

Set up an n-order uncertain system with disturbance as follows

$$x^{(n)} = f\left(x, \dot{x}, \cdots, x^{(n-1)}\right) + W(t) + bu \tag{1}$$

Its state space equation is

$$\begin{cases} \dot{x}_1 = x_2 \\ \vdots \\ \dot{x}_{n-1} = x_n \\ \dot{x}_n = f\left(x, \dot{x}, \cdots, x^{(n-1)}\right) + W(t) + bu \\ y = x_1 \end{cases} \tag{2}$$

In the formula, x represents the system state variable, u denotes the system state input, b signifies the input gain, $f\left(x, \dot{x}, \cdots, x^{(n-1)}\right)$ stands for the known disturbance of the system, and $W(t)$ indicates the unknown disturbance

Let $a(x,t) = f\left(x, \dot{x}, \cdots, x^{(n-1)}\right) + W(t)$ be the total disturbance of the system, thus the input of the controller is chosen as

$$u = u_0 - \frac{a(x,t)}{b} \tag{3}$$

ISSN: 2414-1895 DOI: 10.6919/ICJE.202603_12(3).0028

(1) n-order tracking differentiator

For an n-order system, an n-order tracking differentiator is generally used, and its standard form is

$$\begin{cases} \dot{z}_{11} = z_{12} \\ \vdots \\ \dot{z}_{1n-1} = z_{1n} \\ \dot{z}_{1n} = -r^n \mathrm{fal}\left(\mathrm{z}_{11} - v, \alpha_0, \delta_0\right) \end{cases} \tag{4}$$

In the formula, z_{11} represents the tracking signal of the given signal v, z_{12} to z_{1n} represent the various order derivatives of this signal, r is an adjustable parameter that determines the tracking speed of the differentiator, and the specific form of the fal nonlinear function is

$$\mathrm{fal}\left(\mathrm{x}, \alpha, \delta\right) = \begin{cases} x/\delta^{1-\alpha}, & |x| \le \delta \\ |x|^{\alpha} \operatorname{sgn}(x), & |x| > \delta \end{cases} \tag{5}$$

(2) n+1-order extended state observer

For the n-order uncertain system with disturbances shown in equation (1), an n+1-order extended state observer is designed, and its standard form is

$$\begin{cases} \dot{z}_{21} = z_{22} - \beta_{01}\mathrm{fal}\left(z_{21} - x_1, \alpha_1, \delta_1\right) \\ \dot{z}_{22} = z_{23} - \beta_{02}\mathrm{fal}\left(z_{21} - x_1, \alpha_2, \delta_2\right) \\ \vdots \\ \dot{z}_{2\mathrm{n}} = z_{2\mathrm{n}+1} - \beta_{0\mathrm{n}}\mathrm{fal}\left(z_{21} - x_1, \alpha_{\mathrm{n}}, \delta_{\mathrm{n}}\right) + b_0 u \\ \dot{z}_{2\mathrm{n}+1} = -\beta_{0\mathrm{n}+1}\mathrm{fal}\left(z_{21} - x_1, \alpha_{\mathrm{n}+1}, \delta_{\mathrm{n}+1}\right) \end{cases} \tag{6}$$

In the formula, z_{21} represents the tracking value of the system output, z_{22} to $z_{2\mathrm{n}}$ represent the various order differentials of the signal, z_{2n+1} represents the estimated value of the total system disturbance, and β_{01} to $\beta_{0\mathrm{n}+1}$ represent the various order gains of the observer.

(3) Linear state error feedback control law

Linear state error feedback control laws come in various forms, with the linear error combination form being commonly used. Its standard form is as follows:

$$\begin{cases} u_0 = \beta_1\mathrm{fal}\left(\mathrm{z}_{11} - z_{21}, \alpha, \delta\right) + \cdots + \beta_{\mathrm{n}}\mathrm{fal}\left(z_{1\mathrm{n}} - z_{2\mathrm{n}}, \alpha, \delta\right) \\ u = u_0 - \dfrac{z_{2\mathrm{n}+1}}{\mathrm{b}_0} \end{cases} \tag{7}$$

3. Design of Current Loop Active Disturbance Rejection Controller

3.1 Linear Expansion State Observer

The current differential equation for a permanent magnet synchronous motor is.

ISSN: 2414-1895 DOI: 10.6919/ICJE.202603_12(3).0028

$$\begin{cases} \dfrac{\mathrm{d}i_{\mathrm{d}}}{\mathrm{d}t} = \dfrac{u_{\mathrm{d}}}{L_{\mathrm{d}}} - \dfrac{R_{\mathrm{s}} i_{\mathrm{d}}}{L_{\mathrm{d}}} + \dfrac{\omega L_{\mathrm{q}} i_{\mathrm{q}}}{L_{\mathrm{d}}} \\ \dfrac{\mathrm{d}i_{\mathrm{q}}}{\mathrm{d}t} = \dfrac{u_{\mathrm{q}}}{L_{\mathrm{q}}} - \dfrac{R_{\mathrm{s}} i_{\mathrm{q}}}{L_{\mathrm{q}}} - \dfrac{\omega L_{\mathrm{d}} i_{\mathrm{d}}}{L_{\mathrm{q}}} - \dfrac{\omega \psi_{\mathrm{f}}}{L_{\mathrm{q}}} \end{cases} \tag{8}$$

For ease of design, the current values of the permanent magnet synchronous motor are normalized. The normalized q-axis current differential equation is

$$\frac{\mathrm{d}i_{\mathrm{q}}^{*}}{\mathrm{d}t} = \frac{u_{\mathrm{q}}}{L_{\mathrm{q}} i_{\mathrm{qN}}} - \frac{R i_{\mathrm{q}}^{*}}{L_{\mathrm{q}}} - \frac{\omega \psi_{\mathrm{f}}}{L_{\mathrm{q}} i_{\mathrm{qN}}} - \omega i_{\mathrm{d}}^{*} \tag{9}$$

In the formula, $i_{\mathrm{q}} = i_{\mathrm{qN}} \cdot i_{\mathrm{q}}^{*}$ and i_{qN} represent the rated currents of the permanent magnet synchronous motor, and i_{q}^{*} denotes the q-axis current after being per-unit normalized.

In the current loop of a permanent magnet synchronous motor, the output of the current controller needs to pass through a power circuit to output three-phase voltage in order to drive the three-phase motor to operate. The power circuit includes a rectifier circuit, a filter circuit, and an inverter circuit. The operation of the power circuit has a certain delay, which can be equivalent to a first-order inertia element:

$$\frac{K_{\mathrm{pwm}}}{T_{\mathrm{pwm}} s + 1} \tag{10}$$

In the formula, K_{pwm} represents the voltage amplification factor of the inverter, and T_{pwm} denotes the delay time of the entire power circuit.

Taking into account the inertia component of the aforementioned current loop, a third-order linear extended state observer is designed in the current controller. Laplace transform is applied to equation (4)

$$s i_{\mathrm{q}}^{*}(s) = \frac{u_{\mathrm{q}}(s)}{L i_{\mathrm{qN}}} - \frac{R i_{\mathrm{q}}^{*}(s)}{L} - \frac{\omega \psi_{\mathrm{f}}}{L i_{\mathrm{qN}}} - \omega i_{\mathrm{d}}^{*}(s) \tag{11}$$

Substituting formula (10) into formula (11) yields

$$s i_{\mathrm{q}}^{*}(s) = \frac{1}{L i_{\mathrm{qN}}} \frac{K_{\mathrm{pwm}}}{T_{\mathrm{pwm}} s + 1} u_{\mathrm{q}}^{*}(s) - \frac{R i_{\mathrm{q}}^{*}(s)}{L} - \frac{\omega \psi_{\mathrm{f}}}{L i_{\mathrm{qN}}} - \omega i_{\mathrm{d}}^{*}(s) \tag{12}$$

The above formula can be transformed into the following form:

$$s^{2} i_{\mathrm{q}}^{*}(s) = b u_{\mathrm{q}}^{*}(s) - a_{0} s i_{\mathrm{q}}^{*}(s) - a_{1} i_{\mathrm{q}}^{*}(s) - \frac{s\omega \psi_{\mathrm{f}}}{L i_{\mathrm{qN}}} - \frac{\omega \psi_{\mathrm{f}}}{L T_{\mathrm{pwm}} i_{\mathrm{qN}}} - \omega s i_{d}^{*} - \frac{\omega i_{\mathrm{d}}^{*}}{T_{\mathrm{pwm}}} \tag{13}$$

ISSN: 2414-1895 DOI: 10.6919/ICJE.202603_12(3).0028

In the equation, $a_0 = \frac{R}{L} + \frac{1}{T_{\text{pwm}}}$, $a_1 = -\frac{R}{LT_{\text{pwm}}}$, $b = \frac{K_{\text{pwm}}}{LT_{\text{pwm}} i_{\text{qN}}}$.

Next, we can obtain it through the Laplace inverse transform

$$\ddot{i}_{\text{q}}^{*} = \frac{K_{\text{pwm}}}{LT_{\text{pwm}} i_{\text{qN}}} u_{\text{q}}^{*} - \left(\frac{R}{L} + \frac{1}{T_{\text{pwm}}} \right) \dot{i}_{\text{q}}^{*} - \frac{R}{LT_{\text{pwm}}} i_{\text{q}}^{*} - \frac{\dot{\omega}\psi_{\text{f}}}{Li_{\text{qN}}} - \frac{\omega\psi_{\text{f}}}{LT_{\text{pwm}} i_{\text{qN}}} - \dot{\omega} i_{\text{d}}^{*} - \frac{\omega i_{\text{d}}^{*}}{T_{\text{pwm}}} \tag{14}$$

Let $a(t) = -\frac{\dot{\omega}\psi_{\text{f}}}{Li_{\text{qN}}} - \frac{\omega\psi_{\text{f}}}{LT_{\text{pwm}} i_{\text{qN}}} - \dot{\omega} i_{\text{d}}^{*} - \frac{\omega i_{\text{d}}^{*}}{T_{\text{pwm}}}$ be the expansion of the first-order state variable, and let $x_3 = a(t)$ be such that a third-order extended state observer can be obtained:

$$\begin{cases} e = z_1 - i_{\text{q}}^{*} \\ \dot{z}_1 = z_2 - \beta_1 e \\ \dot{z}_2 = -a_0 z_2 - a_1 z_1 + z_3 + b u_{\text{q}}^{*} - \beta_2 e \\ \dot{z}_3 = -\beta_3 e \end{cases} \tag{15}$$

As shown in Figure 1, it is the structural diagram of the extended state observer, where z_2 follows the derivative of i_q^*. When $t \to \infty$, the extended state observer has

$$z_3 \to a(t) = -\frac{\dot{\omega}\psi_{\text{f}}}{Li_{\text{qN}}} - \frac{\omega\psi_{\text{f}}}{LT_{\text{pwm}} i_{\text{qN}}} - \dot{\omega} i_{\text{d}} - \frac{\omega i_{\text{d}}}{T_{\text{pwm}}} \tag{16}$$

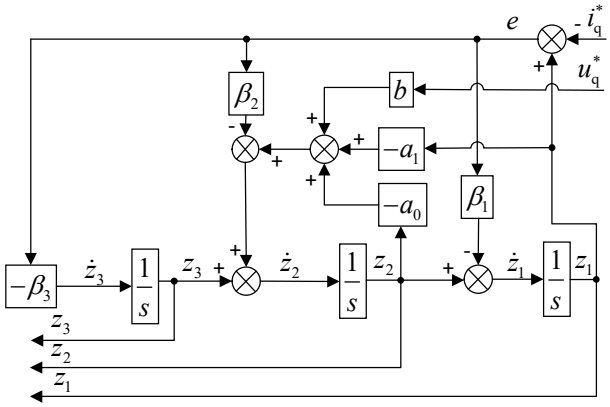

Figure 1. Structure diagram of current loop linear extended state observer

By incorporating the aforementioned linear extended state observer into the current loop of the motor, the system block diagram is illustrated in Figure 2.

ISSN: 2414-1895 DOI: 10.6919/ICJE.202603_12(3).0028

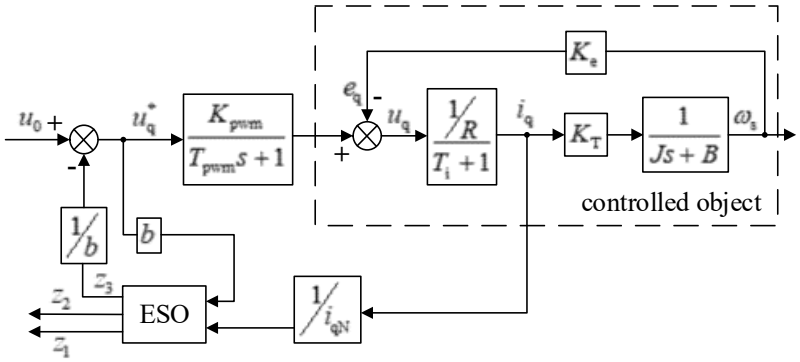

Figure 2. Current loop structure with extended state observer

We can obtain from Figure 2 that

$$u_q^* = u_0 - \frac{z_3}{b} \tag{17}$$

By substituting equations (17) and (16) into equation (14), we obtain

$$\ddot{i}_q^* = \frac{K_{pwm}}{LT_{pwm}i_{qN}}u_0 - \left(\frac{R}{L} + \frac{1}{T_{pwm}}\right)\dot{i}_q^* - \frac{R}{LT_{pwm}}i_q^* \tag{18}$$

Then, by performing the Laplace transform, we can obtain the system as

$$i_q^*(s) = \frac{1}{i_{qN}}\frac{K_{pwm}}{T_{pwm}s+1}\frac{1}{Ls+R}u_0(s) \tag{19}$$

3.2 Design of State Error Feedback Law

Based on the linear extended state observer in the previous section, ignoring the influence of back electromotive force and mutual coupling between D and Q axes, the control block diagram of the current loop transfer function is obtained as shown in Figure 3.

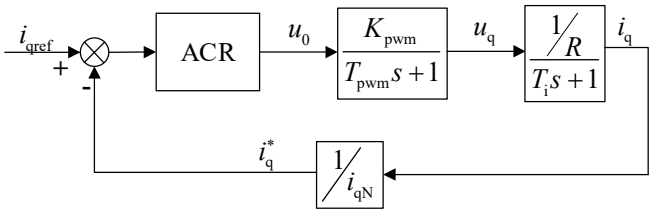

Figure 3. Simplified transfer function control block diagram of current loop

The PI controller of the current loop is set to be of Type I. Its open-loop transfer function and closed-loop transfer function are as follows:

$$W_{op}(s) = \frac{K}{s(Ts+1)} \tag{20}$$

ISSN: 2414-1895 DOI: 10.6919/ICJE.202603_12(3).0028

$$W_{\mathrm{cl}}(s)=\frac{\dfrac{K}{s(Ts+1)}}{1+\dfrac{K}{s(Ts+1)}}=\frac{1}{\dfrac{T}{K}s^2+\dfrac{1}{K}s+1} \tag{21}$$

Rewriting the above expression into a standard second-order system expression:

$$G(s)=\frac{1}{T_{\mathrm{c}}^2s^2+2\xi T_{\mathrm{c}}s+1} \tag{22}$$

In the formula, T_{c} represents the time constant of the second-order system, ξ denotes the damping coefficient, and $\xi=0.707$ is selected based on general experience.

Combining equation (21) with equation (22), we obtain

$$K=\frac{1}{2T} \tag{23}$$

Due to the Type I system, it can be known from $\sigma=4.3\%$, $\omega_{\mathrm{c}}=0.455/T$, and $\gamma=65.5^{\circ}$ that the closed-loop bandwidth of the system is $1/\sqrt{2}T$.

Since the servo system employs a first-order low-pass filter in current setting and current feedback, its transfer function is

$$\frac{1}{T_{\mathrm{fi}}s+1} \tag{24}$$

In the formula, A represents the time constant of the filter.

The system block diagram with the filtering link added is shown below:

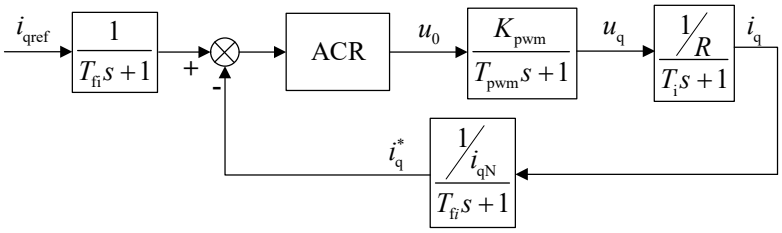

Figure 4. Current loop control block diagram considering filter

Both the inverter and filter links are small-inertia components of the system. By transforming the system block diagram through transfer, the feedback is converted into unit feedback, as shown in Figure 5a. By adding the time constants of the two small-inertia components mentioned above, we can obtain their equivalent first-order inertia component as follows:

$$T_{\sum i}=T_{\mathrm{pwm}}+T_{\mathrm{fi}} \tag{25}$$

ISSN: 2414-1895 DOI: 10.6919/ICJE.202603_12(3).0028

Combine equation (10) and equation (24) to obtain

$$\omega_{\mathrm{ci}} \le \frac{1}{3}\sqrt{\frac{1}{T_{\mathrm{pwm}}T_{\mathrm{fi}}}} \tag{26}$$

In the formula, A represents the open-loop cutoff frequency of the current loop. The control block diagram of the current loop after merging is shown in Figure 5b. The control object after merging is

$$G_{\mathrm{pi}}(s) = \frac{K_{\mathrm{pwm}} \big/ Ri_{\mathrm{qN}}}{\left(T_{\sum i}+1\right)\left(T_{\mathrm{i}}+1\right)} \tag{27}$$

The current controller employs PI control combined with a state error feedback control law, and its transfer function is

$$W_{\mathrm{ACR}} = \frac{K_{\mathrm{i}}\left(\tau_{\mathrm{i}}s+1\right)}{\tau_{\mathrm{i}}s} \tag{28}$$

To reduce the system order, we can obtain the result by multiplying equation (28) with equation (27)

$$W_{\mathrm{opi}}(s) = W_{\mathrm{ACR}}(s)G_{\mathrm{pi}}(s) = \frac{K_{\mathrm{i}}\left(\tau_{\mathrm{i}}s+1\right)}{\tau_{\mathrm{i}}s}\frac{K_{\mathrm{pwm}} \big/ Ri_{\mathrm{qN}}}{\left(T_{\sum i}s+1\right)\left(T_{\mathrm{i}}s+1\right)} = \frac{K_{\mathrm{i}}K_{\mathrm{pwm}} \big/ Ri_{\mathrm{qN}}}{\tau_{\mathrm{i}}s\left(T_{\sum i}s+1\right)} \tag{29}$$

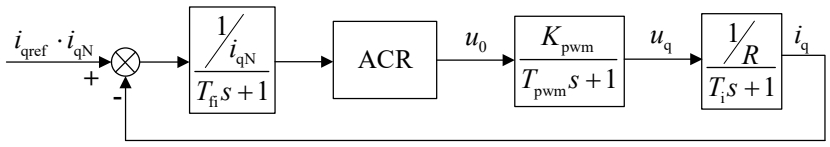

(a) Convert to unity negative feedback

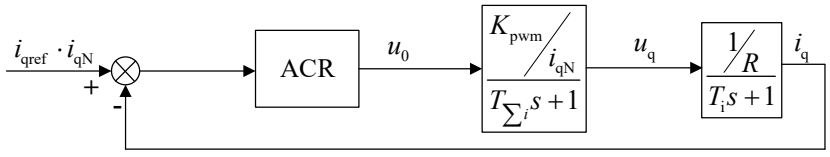

(b) Processing of small inertia links

Figure 5. Equivalent transformation diagram of current loop control block diagram

From the above process, it can be seen that the open-loop transfer function of the system is

ISSN: 2414-1895 DOI: 10.6919/ICJE.202603_12(3).0028

$$W_{\text{opi}}(s)=\frac{K_{\text{I}}}{s\left(T_{\sum i}s+1\right)} \tag{30}$$

where K_{i} is

$$K_{\text{I}}=\frac{K_{\text{i}}K_{\text{pwm}}}{Ri_{\text{qN}}\tau_{\text{i}}}=\frac{K_{\text{i}}K_{\text{pwm}}}{Ri_{\text{qN}}T_{\text{i}}}=\frac{K_{\text{i}}K_{\text{pwm}}}{Li_{\text{qN}}} \tag{31}$$

According to equation (29), the proportional parameter in PI control is

$$K_{\text{i}}=\frac{K_{\text{I}}Li_{\text{qN}}}{K_{\text{pwm}}}=\frac{Li_{\text{qN}}}{2K_{\text{pwm}}T_{\sum i}} \tag{32}$$

Using a PI controller designed based on the Type I scheme, the control parameters and performance indicators are as follows:

$$\tau_{\text{i}}=T_{\text{e}} \tag{33}$$

$$\delta=4.3\% \tag{34}$$

$$\omega_{\text{bi}}=\frac{1}{\sqrt{2}T_{\sum i}} \tag{35}$$

$$\omega_{\text{ci}}=\frac{0.455}{T_{\sum i}} \tag{36}$$

$$\gamma=65.5^{\circ} \tag{37}$$

4. Performance Analysis of Current Loop

4.1 Dynamic Performance Analysis of Current Loop

Based on the analysis in the previous section, the structural block diagram of the current loop controller utilizing active disturbance rejection controller (ADRC) technology is illustrated in Figure 6. The entire current loop control system comprises the ADRC, control object, PWM, inverter, and current feedback link. Firstly, in practical applications, there are numerous disturbances during the current feedback process, necessitating the use of a filter to eliminate these disturbances. However, the filter introduces phase lag, which impacts the dynamic performance of the system. Secondly, PWM and inverter are equivalently represented as a first-order small inertia link. Reducing the time constant of this link can also enhance the system's dynamic performance.

ISSN: 2414-1895 DOI: 10.6919/ICJE.202603_12(3).0028

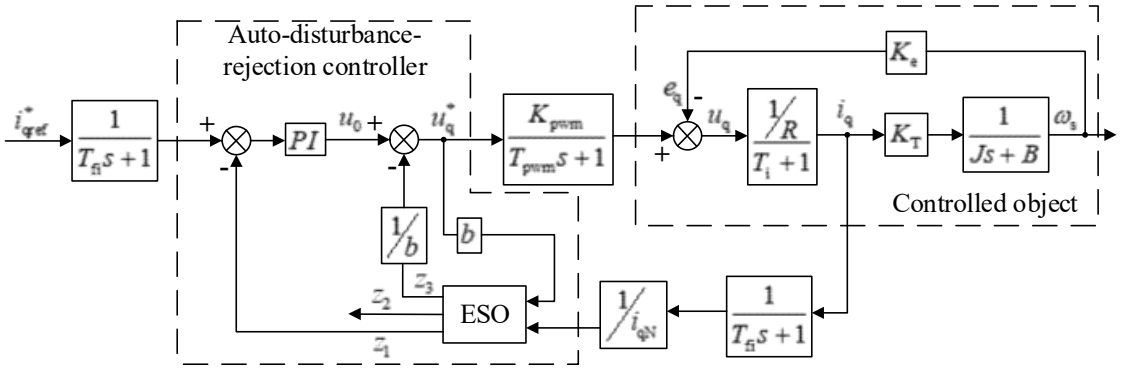

Figure 6. Current loop control block diagram

(1) Current feedback

In the servo industry, the typical current feedback involves using a Hall sensor to convert the current value into a voltage value, which is then fed into a sampling circuit. The voltage value is converted to a range of 0 to 3.3V before being sent to the AD conversion module within the digital processing chip. The entire processing involves multiple conversion steps, making the voltage value susceptible to external interference. This can lead to distortion of the variable before it undergoes AD conversion. Additionally, the built-in AD sampling section of common digital processing chips typically has low accuracy, generally only 10 to 11 bits. A combination of these factors significantly affects the accuracy of current feedback, thereby greatly impacting the control accuracy of the entire servo system.

To address the aforementioned issues, a separate AD sampling chip, such as a delta-sigma ADC sampling chip, can be employed. In traditional ADCs, analog signals are sampled at a certain sampling frequency and then divided into continuous discrete points in a multi-stage processor before being output as digital signals. This process introduces quantization error noise. In delta-sigma ADC sampling chips, delta-sigma modulation is used. The first step of this modulation method is delta modulation, in which the change value of the signal is encoded without using absolute values to represent it. The encoding result forms a pulse stream, rather than a digital stream as in pulse code modulation. In delta-sigma modulation, the accuracy of modulation is improved by passing the digital output through a 1-bit DAC and adding the generated analog signal to the input signal (the signal before delta modulation), thereby reducing the error introduced by delta modulation.

Both ADCs and DACs can utilize delta-sigma modulation. The delta-sigma ADC first encodes the analog signal using high-frequency delta-sigma modulation, and then applies a digital filter to form a high-resolution but low-sampling-frequency digital output. The delta-sigma DAC encodes the high-resolution digital input signal into a low-resolution but high-sampling-frequency signal, which is mapped to a voltage and then smoothed using an analog filter. In both cases, temporarily using a lower-resolution signal can simplify circuit design and improve efficiency.

The expression for the filter in the delta-sigma ADC sampling chip is selected as

$$G(z)=\left(\frac{1}{DR}\times\frac{1-z^{-DR}}{1-z^{-1}}\right)^{N}=\left(\frac{1}{DR}\times\frac{1}{1-z^{-1}}\times 1-z^{-DR}\right)^{N} \tag{38}$$

In the formula, DR represents the sampling frequency, and N denotes the order. Generally, a 3rd-order filter can achieve good filtering effects and obtain the most accurate current sampling.

The delta-sigma modulator generates a pulse stream, where the frequency f of the pulses in the pulse stream is proportional to the analog voltage input v, i.e., $f = k \cdot v$, where k is a constant. The feedback

ISSN: 2414-1895 DOI: 10.6919/ICJE.202603_12(3).0028

loop monitors the integral of v. When the integral increment is Δ, this increment T is represented by the integral waveform crossing the threshold, and T subtracts Δ from the integral of v, so that the combined waveform remains between T and $T-\Delta$.

The counter sums the number of pulses occurring in the predetermined period P, so that the sum Σ equals $P \cdot f = k \cdot P \cdot v$. Under the given conditions, $k \cdot P$ is selected such that Σ contains both v and the already selected coefficients. Since P can take any value, delta-sigma modulation can theoretically select any desired resolution or accuracy.

(2) PWM duty cycle dual update

From the design of the state error feedback law, it can be known that after the current loop system is tuned into a typical Type I system, the open-loop transfer time constant of the current loop is K_{pwm}, which consists of two parts: one is the delay of the PWM and inverter, and the other is the time constant of the filtering link. Both parts are related to the switching frequency of the switch tube. Increasing the switching frequency of the switch tube can effectively reduce the time constant and the rise time of the current loop, and expand the bandwidth of the system, but the switching frequency of the switch tube cannot be infinitely increased. How to maximize the system bandwidth at a certain switching frequency is also a problem worth studying. The update method of the PWM duty cycle can be changed to reduce the delay of the PWM and inverter links, thereby improving the bandwidth of the current loop.

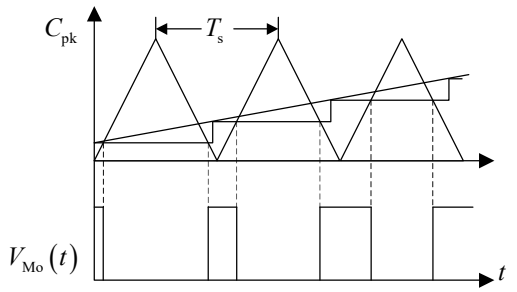

(a) Single update of PWM

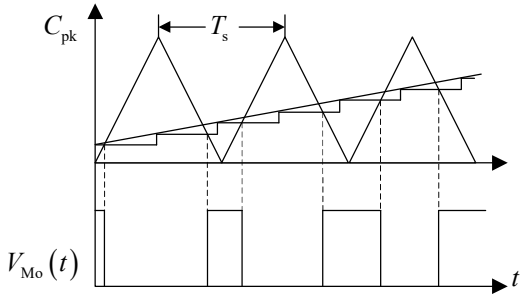

(b) PWM double update

Figure 7. Model of digital PWM

The PWM single update mode is illustrated in Figure 7(a). From Figure 7(a), it can be noticed that the update of the comparison register is only executed at the beginning of the modulation period, that is, when the counter value equals zero. This update mode is called the single update mode. There is a delay in this mode, because in the single update mode, the modulator responds to any disturbance only after the modulation period, thus resulting in a delay. This delay effect varies among different analog modulators, where the response to disturbance takes effect during the modulation period. Therefore, the digital PWM can be modeled using the sample-and-hold effect. The delay of the single update mode is equal to the modulation period.

ISSN: 2414-1895 DOI: 10.6919/ICJE.202603_12(3).0028

In single update mode, the delay between PWM and inverter is

$$T_{\text{pwm1}} = 1.5T_{\text{s}} \tag{39}$$

The PWM dual update mode is illustrated in Figure 7(b). The PWM duty cycle update moments for dual update occur when the counter equals the peak value and when the counter equals zero. In the dual update mode, the register is updated twice per modulation cycle. Therefore, the response to interference takes effect within half of the modulation cycle. The advantage of the dual update mode over the single update mode lies in the fact that the delay effect is reduced to half that of the single update mode. Reducing the delay effect can improve closed-loop performance, and the dual update mode does not increase the requirements for computation and memory.

In dual update mode, the delay between PWM and the inverter is

$$T_{\text{pwm2}} = 0.75T_{\text{s}} \tag{40}$$

Combining equation (36) and equation (37), it can be seen that when using PWM single update, the total system delay is

$$T_{\sum i1} = T_{\text{pwm1}} + T_{\text{oi}} = 1.5T_{\text{s}} + \frac{T_{\text{s}}}{\pi} \approx 1.818T_{\text{s}} \tag{41}$$

Meanwhile, combining with the design of the current loop state feedback control law, it can be known that the bandwidth of the current loop system at this time is

$$\omega_{\text{bi1}} = \frac{1}{\sqrt{2}T_{\sum \text{i1}}} \approx \frac{1}{\sqrt{2} \times 1.818T_{\text{s}}} \approx \frac{0.3890}{T_{\text{s}}} \tag{42}$$

When using PWM dual update, the total system delay is

$$T_{\sum i2} = T_{\text{pwm2}} + T_{\text{oi}} = 0.75T_{\text{s}} + \frac{T_{\text{s}}}{\pi} \approx 1.068T_{\text{s}} \tag{43}$$

At this moment, the bandwidth of the current loop system is

$$\omega_{\text{bi2}} = \frac{1}{\sqrt{2}T_{\sum i2}} \approx \frac{1}{\sqrt{2} \times 1.068T_{s}} \approx \frac{0.6622}{T_{s}} \tag{44}$$

Based on the above comparison, it can be seen that the bandwidth of the current loop has been significantly improved after adopting PWM dual update.

ISSN: 2414-1895 DOI: 10.6919/ICJE.202603_12(3).0028

4.2 Analysis of Disturbance Resistance Performance of Current Loop

Based on the analysis in the previous section, it can be seen that the bandwidth of the current loop after adopting PWM dual update is ω_{bi2}, and parameter $\omega_0 = 5 \sim 10\omega_{bi2}$ is selected based on experience. The corresponding parameters for the extended state observer are

$$\beta_1 = 3\omega_0, \beta_2 = 3\omega_0^2, \beta_3 = \omega_0^3 \tag{45}$$

According to equation (15), the characteristic equation of the linear extended state observer is

$$\lambda(s) = s^3 + (\beta_1 + a_0)s^2 + (\beta_2 + \beta_1 a_0 + a_1)s + \beta_3 \tag{46}$$

The Routh table of the system is

$$\begin{array}{ccc} s^3 & 1 & \beta_2 + \beta_1 a_0 + a_1 \\ s^2 & \beta_1 + a_0 & \beta_3 \\ s^1 & \dfrac{(\beta_2 + \beta_1 a_0 + a_1)(\beta_1 + a_0) - \beta_3}{\beta_1 + a_0} & \\ s^0 & \beta_3 & \end{array} \tag{47}$$

By substituting the value of equation (45) into the above equation, we obtain

$$\frac{(\beta_2 + \beta_1 a_0 + a_1)(\beta_1 + a_0) - \beta_3}{\beta_1 + a_0} = \frac{(3\omega_0 a_0 + a_1)(3\omega_0 + a_0) + 3\omega_0^2 a_0 + 8\omega_0^3}{3\omega_0 + a_0} > 0 \tag{48}$$

Selecting the above parameters can ensure the stability of the observation system.

During the operation of the servo system, if the acceleration or deceleration is too large, or if the system operates under heavy load conditions, the current value i_q in the system will be relatively high, causing the temperature of the permanent magnet synchronous motor to rise. This leads to significant changes in the resistance and inductance values of the motor, and the model of the system will also undergo corresponding changes. Assuming the changes are as follows:

$$R = R_0 + \Delta R \tag{49}$$

$$L = L_0 + \Delta L \tag{50}$$

In the formula, R_0 and L_0 represent the original resistance and inductance values of the system, respectively, while ΔR and ΔL represent the changes in resistance and inductance values, respectively. By substituting equations (49) and (50) into equation (8), we obtain the system model after the changes:

ISSN: 2414-1895 DOI: 10.6919/ICJE.202603_12(3).0028

$$\left(L_0+\Delta L\right)\frac{\mathrm{d}i_\mathrm{q}}{\mathrm{d}t}=u_\mathrm{q}-\left(R_0+\Delta R\right)i_\mathrm{q}-\omega_0 L_0 i_\mathrm{d}-\omega\psi_\mathrm{f} \tag{51}$$

The output of the linear extended state observer is

$$\dddot{i}_\mathrm{q}^*=\frac{K_\mathrm{pwm}}{L_0 T_\mathrm{pwm} i_\mathrm{qN}}u_\mathrm{q}^*-\left(\frac{R_0}{L_0}+\frac{1}{T_\mathrm{pwm}}\right)\ddot{i}_\mathrm{q}^*-\frac{R_0}{L_0 T_\mathrm{pwm}}\dot{i}_\mathrm{q}^*-a\left(t\right) \tag{52}$$

Where $a\left(t\right)$ is

$$a\left(t\right)=-\frac{\Delta R}{L_0}\ddot{i}_\mathrm{q}^*-\frac{\Delta R}{L_0 T_\mathrm{pwm}}\dot{i}_\mathrm{q}^*-\frac{\Delta L}{L_0}\dddot{i}_\mathrm{q}^*-\frac{\Delta L}{L_0 T_\mathrm{pwm}}\ddot{i}_\mathrm{q}^*-\frac{\dot{\omega}\psi_\mathrm{f}}{L_0 i_\mathrm{qN}}-\frac{\omega\psi_\mathrm{f}}{L_0 T_\mathrm{pwm} i_\mathrm{qN}}-\dot{\omega}i_\mathrm{d}^*-\frac{\omega i_\mathrm{d}^*}{T_\mathrm{pwm}} \tag{53}$$

According to the linear extended state observer of equation (16), we can see that

$$z_3\rightarrow a\left(t\right) \tag{54}$$

The controller output is

$$u_q^*=u_0-\frac{z_3}{b} \tag{55}$$

Therefore, we can ultimately obtain:

$$i_q^*\left(s\right)=\frac{1}{i_\mathrm{qN}}\frac{K_\mathrm{pwm}}{T_\mathrm{pwm}s+1}\frac{1}{\left(Ls+R\right)}u_0\left(s\right) \tag{56}$$

When resistance and inductance values change, the extended state observer can mitigate the impact to a certain extent. The specific parameters need to be selected based on the actual engineering situation.

5. Experiment Verification

Considering that traditional servo current loop control systems primarily rely on precise mathematical models of permanent magnet synchronous motors (PMSMs), these systems are sensitive to motor parameter perturbations. To address this issue, this experiment, based on a novel current loop control algorithm, selects two of the most typical electrical parameters of PMSMs: stator resistance and stator inductance parameter perturbations as examples. In the controller, three scenarios are selected for comparative experiments: the motor stator resistance and inductance are set to their actual values, the motor stator resistance is set to 0.5 times its actual value, and the motor stator inductance is set to 0.5 times its actual value. This is done to verify the robustness of the novel current loop control algorithm to internal parameter perturbations of the motor. The dynamic response performance of the novel

ISSN: 2414-1895 DOI: 10.6919/ICJE.202603_12(3).0028

current loop control system is verified by observing the q-axis current response waveform under a sudden change in given load torque.

To verify the dynamic response performance of the novel servo current loop system under uncertain load disturbances, under constant speed conditions, a sudden change in load torque of a permanent magnet synchronous motor was given, and the dq-axis given current and actual current responses were compared. Figure 8 shows the waveform comparison of the dq-axis given current and actual current responses in the current loop system when the motor stator resistance and inductance values are selected as actual values. Figure 8a shows the d-axis (direct axis) current waveform, and Figure 8b shows the q-axis (quadrature axis/torque) current waveform. The motor was operated under no-load and 500r/min conditions. At the 0.5s mark, a sudden increase in rated load was applied to the servo system through the dynamometer controller, and at the 2.0s mark, the rated load was suddenly removed from the servo system. Observing Figure 8a, it can be seen that under the condition where the motor stator resistance and inductance values are selected as actual values in the current loop system, sudden load disturbances have no significant impact on the d-axis current. The actual value of the d-axis current always fluctuates around the given value within a range of ±0.3A. Observing Figure 8b, it can be seen that at the moment of a sudden increase in motor load, the q-axis torque current quickly follows the given target value with almost no overshoot, and the response time is approximately only 20ms. At the moment of a sudden decrease in motor load, the q-axis torque current also quickly follows the given target value with almost no overshoot, and the response time is approximately only 20ms. Furthermore, the actual value of the q-axis torque current fluctuates only within a range of ±0.4A under no-load and rated load conditions. This experimental waveform verifies that the novel servo current loop control system has strong dynamic response capabilities to external load disturbances.

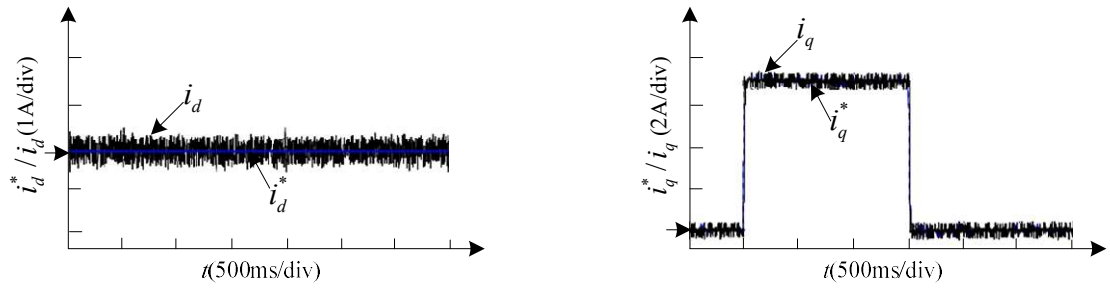

(a) d-axis current (b) q-axis current

Figure 8. Current waveforms of dq axis under the actual values of stator resistance and inductance in the controller (500r/min)

Similarly, the dynamic response performance of the new servo current loop system under uncertain load disturbances at rated speed conditions was verified. As shown in Figure 9, under rated speed conditions (2500r/min), the comparison of the given current and actual current response waveforms on the dq axis in the current loop system with actual values of motor stator resistance and inductance is presented. Figure 9a shows the d-axis (direct axis) current waveform, and Figure 9b shows the q-axis (quadrature axis/torque) current waveform. The motor was operated under no-load and 2500r/min conditions. At the 0.5s mark, a rated load was suddenly applied to the servo system through the dynamometer controller, and at the 2.0s mark, the rated load was suddenly removed from the servo system. Observing Figure 9a, it can be seen that under the condition of selecting actual values for motor stator resistance and inductance in the current loop system, sudden load disturbances have no significant impact on the d-axis current. The actual value of the d-axis current always fluctuates around the given value within a range of ±0.5A, which is slightly larger than that under 500r/min conditions. Observing Figure 9b, it can be seen that at the moment of sudden load increase and

ISSN: 2414-1895 DOI: 10.6919/ICJE.202603_12(3).0028

decrease, the q-axis torque current can quickly follow the given target value with almost no overshoot. The actual value of the q-axis torque current fluctuates only within a range of ±0.5A under both no-load and rated load conditions. This further verifies that the new servo current loop control system has strong dynamic response capabilities to external load disturbances.

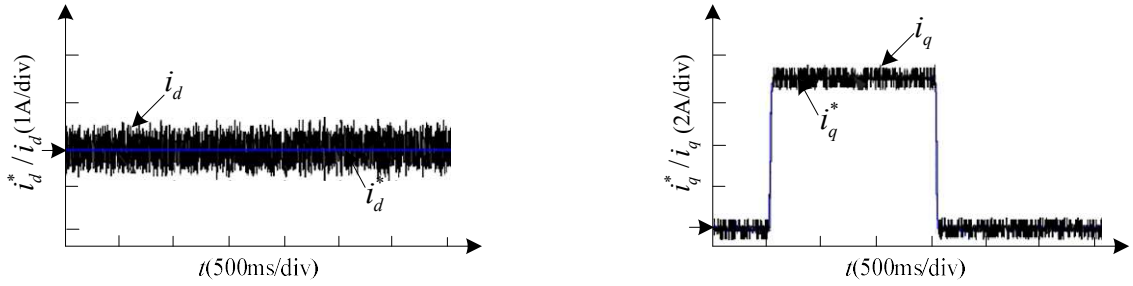

(a) d-axis current (b) q-axis current

Figure 9. Current waveforms of dq axis under the actual values of stator resistance and inductance in the controller(2500r/min)

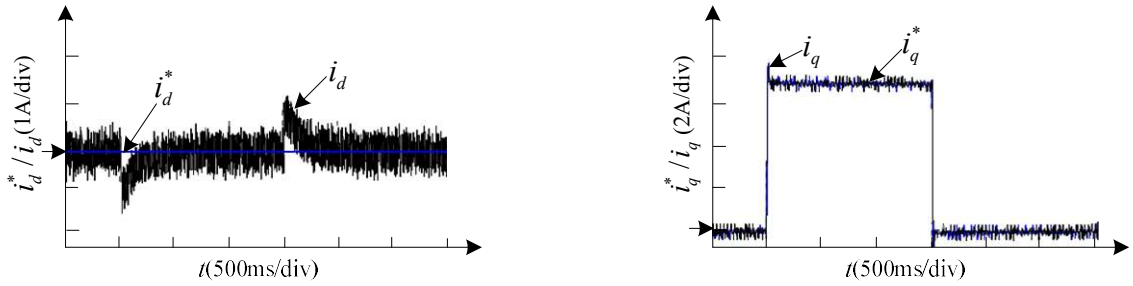

(a) d-axis current (b) q-axis current

Figure 10. Current waveforms of dq axis under 0.5 times the actual value of stator resistance in the controller(500r/min)

To verify the robustness of the new servo current loop system to internal parameter perturbations in the motor, under constant speed conditions, a perturbation of the motor stator resistance parameter was given to the servo system controller, and the dq-axis given current and actual current responses were compared. Figure 10 shows the waveform comparison of the dq-axis given current and actual current responses in the current loop system when the motor stator resistance value is set to 0.5 times the actual value. Figure 10a shows the d-axis (direct axis) current waveform, and Figure 10b shows the q-axis (quadrature axis/torque) current waveform. The motor was operated under no-load and 500r/min conditions. At the 0.5s mark, a rated load was suddenly applied to the servo system through the dynamometer controller, and at the 2.0s mark, the rated load was suddenly removed from the servo system. Observing Figure 10a, it can be seen that under the perturbation of the motor stator resistance parameter in the current loop system, the sudden increase and decrease in load disturbance have a relatively significant impact on the d-axis current. At the moment of sudden load increase, the actual value of the d-axis current fluctuates downward by about -1.5A, and at the moment of sudden load decrease, the actual value of the d-axis current fluctuates upward by about +1.2A. However, the actual value of the d-axis current quickly recovers to a steady state after about 200ms. Considering that the d-axis current has no significant impact on the output torque of the servo system, this disturbance has a minor impact on the servo system. Observing Figure 10b, it can be seen that at the moment of sudden load increase in the given motor, the q-axis torque current has an overshoot of about 1A compared to the condition without parameter perturbation, but it quickly recovers to a steady

ISSN: 2414-1895 DOI: 10.6919/ICJE.202603_12(3).0028

state after only about 10ms. At the moment of sudden load decrease in the given motor, the q-axis torque current also has an overshoot of about 1A compared to the condition without parameter perturbation, and it quickly recovers to a steady state. This experimental waveform verifies that the new servo current loop control system has a certain degree of robustness to motor stator resistance parameter perturbations.

Similarly, given the rated speed condition of the motor (2500r/min), the stator resistance value of the motor in the current loop system is selected to be 0.5 times the actual value. Figure 11 shows the comparison between the dq axis given current and the actual current response waveform under this condition, where Figure 11a shows the d-axis (direct axis) current waveform and Figure 11b shows the q-axis (quadrature axis/torque) current waveform. Comparing Figure 11 and Figure 10, it can be seen that after the speed increases, the perturbation of resistance parameters slightly increases the impact on the d-axis current (the d-axis current fluctuates to around 2A at the moment of load sudden change, and actually recovers to steady state after 500ms), but has no significant effect on the q-axis current. Further verification has shown that the new servo current loop control system has a certain robustness to the perturbation of motor stator resistance parameters.

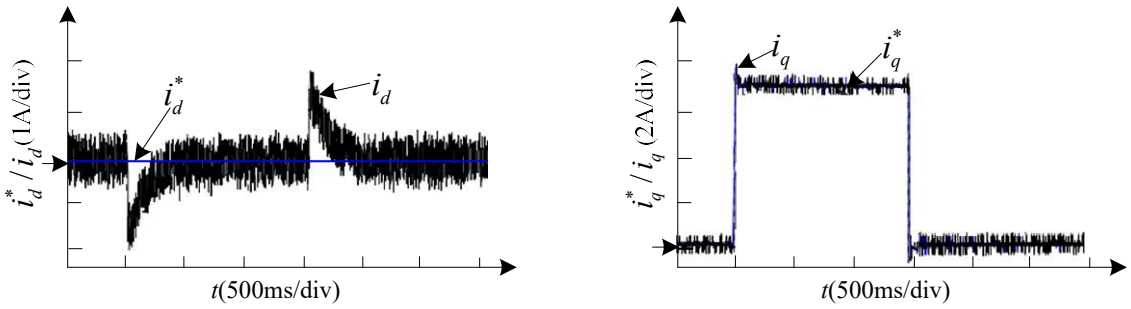

(a) d-axis current (b) q-axis current

Figure 11. Current waveforms of dq axis under 0.5 times the actual value of stator resistance in the controller(2500r/min)

In order to further verify the robustness of the new servo current loop system to internal parameter perturbations of the motor. Under constant speed conditions, the stator inductance parameter of the servo system controller motor is perturbed, and the dq axis given current is compared with the actual current response. As shown in Figure 12, the comparison between the dq axis given current and the actual current response waveform in the current loop system with a stator inductance value of 0.5 times the actual value is presented. Figure 12a shows the d-axis current waveform, and Figure 12b shows the q-axis current waveform. Given the motor operating at no load and 500r/min, at 0.5s, the servo system is given a sudden rated load by the dynamometer controller, and at 2.0s, the servo system is given a sudden rated load to be unloaded. Observing Figure 12a, it can be seen that under the perturbation of the stator inductance parameters in the current loop system, the sudden rise and fall of the load disturbance also has a significant impact on the d-axis current. At the moment of sudden rise of the load, the actual value of the d-axis current fluctuates upward by about+0.8A, and at the moment of sudden fall of the load, the actual value of the d-axis current fluctuates downward by about -0.8A. The fluctuation values of both are reduced compared to the perturbation of the resistance parameters in Figure 11a. Similarly, the actual value of the d-axis current can quickly recover to steady state after about 200ms. Considering that the d-axis current has no significant effect on the output torque of the servo system, the disturbance has a relatively small impact on the servo system. Observing Figure 12b, it can be seen that at the moment of sudden rise and fall of the given motor load, the q-axis torque current is not significantly different from the operating condition without parameter perturbation. Under this parameter perturbation, the q-axis current can also quickly track the target setpoint without overshoot. The experimental waveform verifies that the new servo current

ISSN: 2414-1895 DOI: 10.6919/ICJE.202603_12(3).0028

loop control system has strong robustness to perturbations in the stator inductance parameters of the motor.

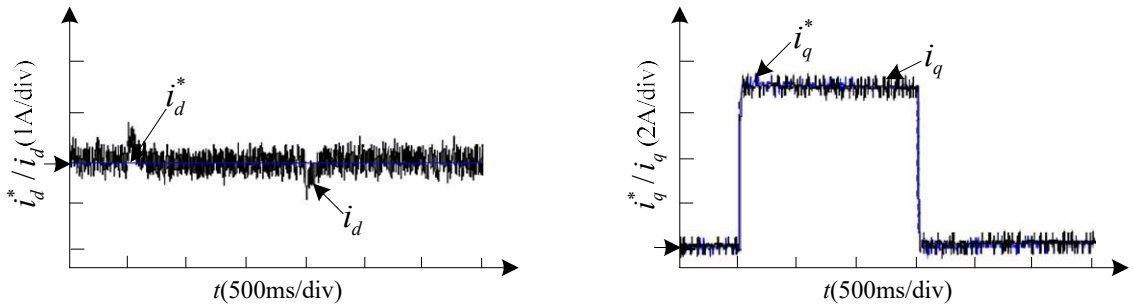

(a) d-axis current (b) q-axis current

Figure 12. Current waveforms of dq axis under 0.5 times the actual value of stator inductance in the controller(500r/min)

Similarly, given the rated speed condition of the motor (2500r/min), the stator inductance value of the motor in the current loop system is selected to be 0.5 times the actual value. Figure 13 shows the comparison of the dq axis given current and actual current response waveforms under this condition, where Figure 13a shows the d-axis current waveform and Figure 13b shows the q-axis current waveform. Comparing Figure 12 and Figure 13, it can be seen that after the speed increases, the perturbation of inductance parameters slightly increases the impact on the d-axis current (the d-axis current fluctuates to around 1A at the moment of load sudden change, and actually recovers to steady state after 200ms), but has no significant effect on the q-axis current. Further validated the robustness of the new servo current loop control system to perturbations in the stator inductance parameters of the motor.

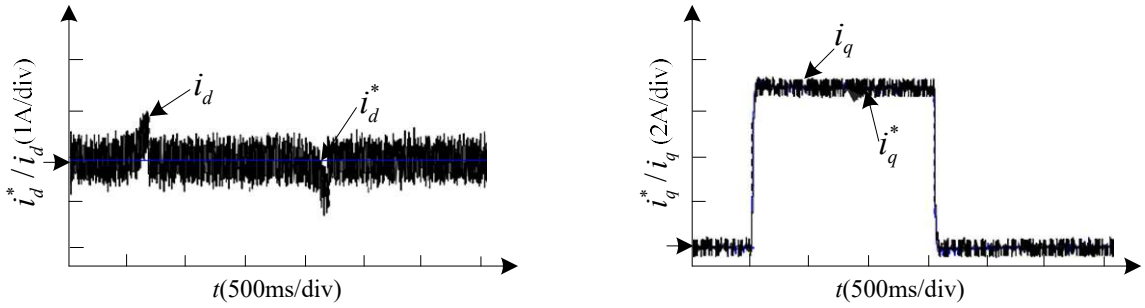

(a) d-axis current (b) q-axis current

Figure 13. Current waveforms of dq axis under 0.5 times the actual value of stator inductance in the controller(2500r/min)

6. Conclusion

This article applies the self disturbance rejection controller to the current loop of a permanent magnet AC servo control system. A current loop self disturbance rejection controller consisting of a linear expansion state observer and a state error feedback rate is designed. After that, the performance of the current loop with the controller is analyzed. In terms of dynamic response, the dynamic performance is improved by improving the current feedback and PWM duty cycle update methods. Finally, the disturbance rejection performance of the current loop is analyzed. The current loop is the most fundamental and important loop in permanent magnet AC servo control systems. The addition of an active disturbance rejection controller to the current loop greatly improves its performance. Experimental results have verified the robustness of the new servo current loop control system to internal parameter perturbations in motors.

ISSN: 2414-1895 DOI: 10.6919/ICJE.202603_12(3).0028

Acknowledgments

The authors thank the editor and anonymous reviewers for their valuable remarks and helpful suggestions. This study was supported by Provincial Research Platform Opening Fund of Yancheng Polytechnic College (YGKF202201).

References

[1] Yan Y, Yang J, Sun Z, et al. Robust speed regulation for PMSM servo system with multiple sources of disturbances via an augmented disturbance observer[J]. IEEE/ASME Transactions on Mechatronics, 2018, 23(2): 769-780.

[2] Xun Q,Wang P L, Li Z X,Cai Z D, Qin H H. Parameter identification of permanent magnet servo system based on recursive least squares method[J]. Journal of Electrotechnology, 2016, 31(17): 161-169.

[3] Yi P, Sun Z, Wang X. Research on PMSM harmonic coupling models based on magnetic co-energy[J]. IET Electric Power Applications, 2019, 13(4): 571-579.

[4] Wang A, Wei S. Sliding mode control for permanent magnet synchronous motor drive based on an improved exponential reaching law[J]. IEEE Access, 2019, 7: 146866-146875.

[5] Zaihidee F M, Mekhilef S, Mubin M. Application of fractional order sliding mode control for speed control of permanent magnet synchronous motor[J]. IEEE Access, 2019, 7: 101765-101774.

[6] Chen S Y, Chiang H H, Liu T S, et al. Precision motion control of permanent magnet linear synchronous motors using adaptive fuzzy fractional-order sliding-mode control[J]. IEEE/ASME Transactions on Mechatronics, 2019, 24(2): 741-752.

[7] Zhao K, Yin T, Zhang C, et al. Sliding mode-based velocity and torque controllers for permanent magnet synchronous motor drives system[J]. The Journal of Engineering, 2019, 2019(23): 8604-8608.

[8] Cao S, Liu J, Yi Y. Non-singular terminal sliding mode adaptive control of permanent magnet synchronous motor based on a disturbance observer[J]. The Journal of Engineering, 2019, 2019(15): 629-634.